AJChE 2009, Vol. 9, No. 1, 16 – 23

One Dimensional Mathematical Model of Re-Ignition Characteristics

Tri Poespowati[a]
[a] Department of Chemical Engineering, The Institute of National Technology, Malang, East Java, Indonesia
E-mail : poespowati@yahoo.com.au

Re-ignition of a wood-based object essentially comprises three overlapping phases; these are the heat-up phase, the extinguishment phase, and the re-heat-up phase. A one-dimensional mathematical model was developed in this study to simulate multiple consecutive ignitions associated with re-ignition process within a porous material. The model focuses on the treatment of heat transfer in porous media that is assumed to be one-dimensional within a homogeneous sample. The effect of porosity is incorporated through the inclusion of an effective thermal conductivity. Our experience indicates that the ignition temperatures and ignition delay times obtained from this approach are in good agreement with relevant experimental data.

Keywords: Model, One Dimensional, Re-Ignition, Porous Material.

INTRODUCTION

Several attempts have been made to model the heat transfer process in porous material (Chase et al., 1970; Sahota and Pagni, 1979; Ahmed and Hurst, 1999; Jiang and Ren, 2001; Fafai and Tien, 1981; Vynnycky and Pop, 1997; Marafie and Vafai, 2001; Tien and Chiang, 1999; Rubin and Schweitzer, 1972; Dlugogorski et al., 2004).

All models that have been described by the above researchers consider some form of Darcian description of the flow within the porous media. However, for problems involving the heat transfer in porous media, it is possible to ignore the Darcy's law but incorporate the effect of porosity into the conductive heat transfer coefficient. For simplicity, this is the approach undertaken in this study. The validity of the approach is evaluated by comparing the predictions with experimental data. A fully implicit finite-volume scheme was employed to discretise the governing equations of the model on a numerical grid. The tri-diagonal matrix algorithm (TDMA) was employed to solve the resulting set of equations. The model is similar to that developed by Dlugogorski and co-workers (2004) where the treatment of porous materials is done by incorporating an effective thermal conductivity that accounts for the porous structure of the material rather than explicitly considering the porosity as a variable in the governing set of equations. Also, in our model the extinguishment phase of the re-ignition process is approximated by applying a negative heat flux to account for the cooling effect of the water spray. As such, there is no need to consider extra equations for the extinguishment phase.

DESCRIPTION OF THE MODEL

The heat transfer is assumed to be one-dimensional within a homogeneous sample. The effect of porosity is incorporated through

the inclusion of an effective thermal conductivity. It is assumed that part of the external heat flux is lost due to re-radiation and convection, the rest is conducted through the sample. Consistent with the experimental set-up, the back-face of the sample is assumed to be insulated (i.e. there is no heat loss from the back-face). This would allow us to consider thermally thick samples although by specifying a temperature at the back-face it is also possible to study thermally thin samples. The governing equations of the model were discretised on a one-dimensional numerical grid and the grid was arranged in a staggered format to avoid numerical instability.

The Mathematical Formulation

The governing equation for the unsteady one-dimensional heat transfer in a general coordinate system, considered in this study, can be written as:

$$\frac{\partial}{\partial t}\left(\rho\, Cp\, T\right)=\frac{1}{\lambda}\frac{\partial}{\partial x}\left(\lambda\, k_{eff}\,\frac{\partial T}{\partial x}\right)+S \quad (1)$$

where is factor of geometry that is equal to 1 for rectangular geometry, the density, *Cp* the specific heat ($Cp = Cp_a + Cp_b\, T$), *x* the space coordinate, *t* time, *T* the local temperature, k_{eff} the effective thermal conductivity ($k_{eff} = k_a + k_b\, T$), and *S* a source term. As can be seen, both thermal conductivity and specific heat of the solid were assumed to be linear functions of the local temperature.

The term on the left hand side of Eq. (1) represents the rate of change of energy stored in the control volume while the first term on the right hand side accounts for heat transfer by diffusion. The initial and boundary condition of Eq. (1) can be expressed as: Initial condition:

at t = 0, T = T_0 (typically 20 ^{0}C) (2)

Boundary condition:

$$x=L \;\rightarrow\; \frac{\partial T}{\partial x}=0;\quad t>0 \qquad \text{Adiabatic} \quad (3)$$

$$x=0 \;\rightarrow$$

$$-k\frac{\partial T}{\partial x}=\dot{q}''-h\left(T-T_a\right)-\sigma\,\varepsilon\left(T^4-T_a^4\right) \quad (4)$$

where *L* is the sample thickness, $\dot{q}''$ is the external heat flux, *h* is the convective heat transfer coefficient, T_a and T_0 the ambient and initial temperatures, the Stefan Boltzmann constant, and the emissivity. The discretised form of the governing equations for the boundary cell at the front-face (surface cell), a typical cell within the grid (grid cell), and the boundary cell at the back-face (bottom cell) can be written as:

Surface cell:

$$\frac{\rho\, Cp\,\frac{\Delta x}{2}}{\Delta t}\left(T_P-T_P^0\right)=\frac{k}{\Delta x}\left(T_E-T_P\right)+\varepsilon\,\dot{q}''-h\left(T_P-T_a\right)-\sigma\,\varepsilon\left(T_P^4-T_a^4\right) \quad (5)$$

$$\left(\frac{1}{2}\rho\, Cp\frac{\Delta x}{\Delta t}+\frac{k_{eff}}{\Delta x}\right)T_P=\frac{k_{eff}}{\Delta x}T_E+\left(\frac{1}{2}\rho\, Cp\frac{\Delta x}{\Delta t}\right)T_P^0+\varepsilon\,\dot{q}''-h\left(T-T_a\right)-\sigma\,\varepsilon\left(T^4-T_a^4\right) \quad (6)$$

$$\rho\, Cp\frac{\left(T_P-T_P^0\right)\Delta x}{\Delta t}=\frac{k_{eff}}{\Delta x}\left(T_E-T_P\right)-\frac{k_{eff}}{\Delta x}\left(T_P-T_W\right) \quad (7)$$

Grid cell:

$$\left(\rho Cp\frac{\Delta x}{\Delta t}+\frac{k_{eff}}{\Delta x}+\frac{k_{eff}}{\Delta x}\right)T_P=\frac{k_{eff}}{\Delta x}T_E+\frac{k_{eff}}{\Delta x}T_W+\rho Cp\frac{\Delta x}{\Delta t}T_P^0 \quad (8)$$

$$\frac{\rho\, Cp\, \frac{\Delta x}{2}}{\Delta t}\left(T_P - T_P^0\right) = \frac{k}{\Delta x}\left(T_W - T_P\right) \quad (9)$$

Bottom cell:

$$\left(\frac{1}{2}\rho\, Cp\frac{\Delta x}{\Delta t} + \frac{k_{eff}}{\Delta x}\right)T_P = \frac{k_{eff}}{\Delta x}T_W + \left(\frac{1}{2}\rho\, Cp\frac{\Delta x}{\Delta t}\right)T_P^0 \quad (10)$$

Where T_P is the temperature at nodal point, T_E is the temperature at nodes to the East, T_W is the temperature at nodes to the West, and T_P^0 is the temperature at nodal point at initial condition. All discretised equations were multiplied by L/k_aT_a where L is the thickness of the sample. Collection of the discretised equations for all cells within the grid forms a set of strongly coupled algebraic equations, which is solved using the tri-diagonal matrix algorithm.

Physical properties

The ambient temperature was horizontally and vertically measured around the mass loss cone calorimeter. It was found that the average ambient temperature was typically 301.15 K. The calculation of effective thermal conductivity was adopted from Chase et al. (1970), and Hostikka and McGrattan (2001); form which is needed in our model:

$$k_{eff} = k_a + k_bT \quad (11)$$

where k_a and k_b are constants.

The thermal property of samples has been summarized in Table 1:

Table 1: *Thermal properties of samples used in this study.*

Sample	Density, kg.m^{-3}	Porosity	$K_{eff} = k_a + k_b T$, kW.m^{-1}.K^{-1}	$Cp = Cp_a + Cp_b T$, kJ.kg^{-1}K^{-1}
Western Red cedar	1462	0.745864	0.00571 + 0.0000468 T	0.1 + 0.0037 T
Radiata pine	1351	0.579645	0.00441 + 0.0000364 T	0.1 + 0.0037 T
River Red gum	1655	0.346928	0.00267 + 0.0000219 T	0.1 + 0.0037 T

RESULTS AND DISCUSSION

The standard staggered grid consisted of a one-dimensional meshes with cells uniformly distributed between the front- and back-faces. Overall, the standard grid comprised of 40 nodes. Several other grids (5, 20, 30, 50, and 60 nodes) were also used to determine the effect of the overall grid resolution on predictions. While the predictions obtained using the coarser grids (i.e. 5, 20, and 30 nodes) were found to be different from those resulting from the standard grid, the difference between the predictions made by the standard and finer grids (i.e. 50 and 60 nodes) were insignificant. As a result, the solutions from the standard grid were considered to be grid independent.

Validation of the Model

As explained above, heat transfer throughout the porous solids examined in this study was assumed to be one-dimensional in a direction normal to the exposed surface. The parameters utilized for all model calculation are listed in Table 2.

Table 2: Property values of model.

Property	Value
h	49.67 $W.K^{-1}.m^{-2}$
t	1 s
T_0	293.15 K
T_a	301.15 K
	0.97
	$5.67.10^{-8}$ $W.m^{-2}.K^{-4}$
$\dot{q}''$	40, 50, 60 $kW.m^{-2}$

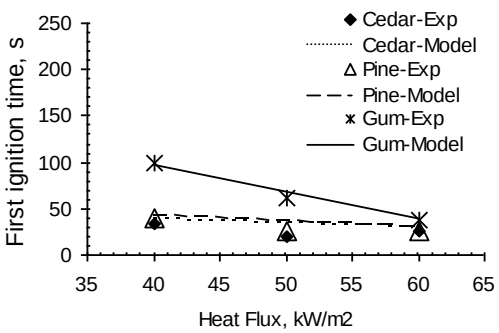

Fig 1. Experiment data and model prediction for the First Ignition time. The data correspond to a 5 s water application time at various levels of incident heat flux.

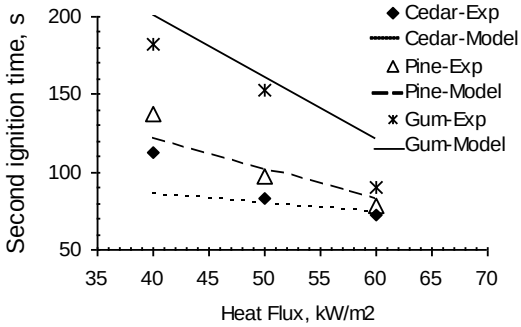

Fig 2. Experiment data and model prediction for the Second Ignition time. The data correspond to a 10 s water application time at various levels of incident heat flux.

Figure 1 illustrates the comparison of the measured and calculated first ignition time for Western Red cedar, Radiata pine, and River Red gum for a 5 s water application time at various heat flux levels. As Fig. 1 indicates, both experimental and predicted data exhibit an inverse linear relationship between the heat flux and ignition time. There is also a remarkably good agreement between the measured and predicted values. One the interesting features of Figure 1 is that, despite their differences, softwood species (i.e. Radiata pine and Cedar) show very similar characteristics whereas the hardwood species (i.e. Gum in this study) exhibit a clearly different characteristic to those of softwoods.

Similarly, Figure 2 shows the plots of the Second Ignition time versus heat flux for the three wood species under investigation. Once again, the predictions of the model are very close to the experimental data and the model has been able to predict the correct trends shown by the experimental data. As can be seen, unlike the case of the First Ignition time, there are some differences between even the softwood species. However, the River Red gum, which is a hardwood species, still demonstrates distinct characteristics.

The next two figures represent the prediction of the Re-ignition delay of wood sample as a function of incident heat flux compare with those of the measured data. While Figure 3 shows the re-ignition time of the River Red gum at different water application times, Figure 4 illustrates those for the three woods species at 10 s water application time. As indicated in Fig. 3, the agreement between model and measured re-ignition delays is not as good as what was observed for the First Ignition time or even the Second Ignition time

(Figures 1 and 2). A similar discrepancy between the measured and predicted data is also observed in Figure 4. This discrepancy is particularly greater at lower levels of heat flux (e.g. H.F. < 50 kW.m^{-2}). The implication of this observation is that the present model should be used with caution when low heat fluxes are studied. However, such low levels of heat flux rarely have any practical importance because the typical heat flux levels for building fires are in excess of 60 kW.m^{-2}. As such, the model presented here can be a very useful tool in studying the re-ignition behavior of solid fuels under fire conditions. The data used in these figures have been extracted from Tables 3 to 6.

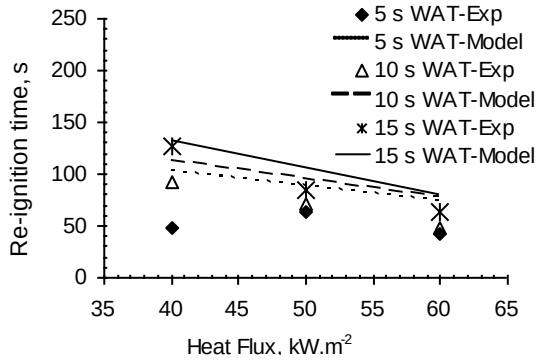

Fig 3. Experiment data and model prediction for River Red gum at different water application times as a function of the incident heat flux.

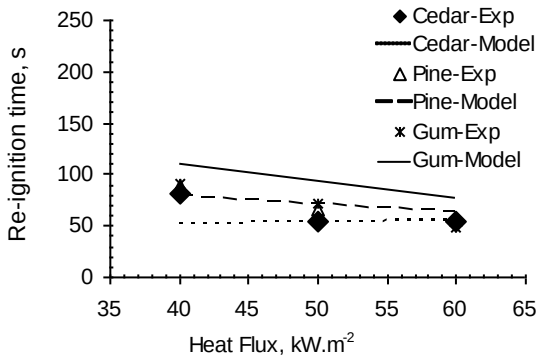

Fig 4. Experiment data and model prediction for the three woods species under investigation. The data correspond to 10 s water application time and various incident heat flux.

Table 3. First Ignition Temperature of wood sample

Sample	WAT	First Ignition Temperature of wood sample, °C.					
		40 kW.m^{-2}		50 kW.m^{-2}		60 kW.m^{-2}	
		Experiment	Model	Experiment	Model	Experiment	Model
Western	5 s	395.75	343.106	321.853	376.222	485.61	446.185
Red cedar	10 s	365.941	338.316	346.967	389.814	380.921	403.106
	15 s	429.936	345.997	370.305	389.814	422.923	419.632
Radiata pine	5 s	416.311	443.928	413.024	481.72	484.004	537.269
	10 s	427.948	445.201	437.669	479.165	387.355	503.308
	15 s	466.042	465.799	420.576	376.222	421.672	516.425
River Red gum	5 s	447.496	398.69	426.855	450.822	441.807	489.346
	10 s	413.311	395.444	459.152	455.551	416.991	488.277
	15 s	409.851	393.821	417.926	453.352	536.709	502.703

Table 4. Second Ignition Temperature of wood sample

Sample	WAT	Second Ignition Temperature of woods sample, °C.					
		40 kW.m^{-2}		50 kW.m^{-2}		60 kW.m^{-2}	
		Experiment	Model	Experiment	Model	Experiment	Model
Western Red cedar	5 s	430.02	343.106	579.095	376.222	414.466	446.185
	10 s	416.542	338.316	365.766	389.814	454.732	403.106
	15 s	472.987	345.997	473.044	389.814	614.85	419.632
Radiata pine	5 s	505.179	443.928	406.956	481.72	355.17	537.269
	10 s	492.257	445.201	519.574	479.165	435.398	503.308
	15 s	340.32	465.799	386.833	376.222	320.858	516.425
River Red gum	5 s	290.293	398.69	436.577	450.822	324.823	489.346
	10 s	398.006	395.444	434.213	455.551	272.75	488.277
	15 s	449.851	393.821	508.558	453.352	367.045	502.703

Table 5. First Ignition Time of wood sample

Sample	WAT	First Ignition Time of woods sample, s.					
		40 kW.m^{-2}		50 kW.m^{-2}		60 kW.m^{-2}	
		Experiment	Model	Experiment	Model	Experiment	Model
Western Red cedar	5 s	33	41	19	25	26	34
	10 s	26	34	21	31	12	19
	15 s	33	40	23	31	18	23
Radiata pine	5 s	40	44	26	31	26	32
	10 s	41	45	25	30	16	22
	15 s	61	68	24	25	19	25
River Red gum	5 s	100	99	62	66	38	41
	10 s	85	85	75	80	34	40
	15 s	75	79	67	73	59	61

Table 6. Second Ignition Time of wood sample

Sample	WAT	Second Ignition Time of woods sample, s.					
		40 kW.m^{-2}		50 kW.m^{-2}		60 kW.m^{-2}	
		Experiment	Model	Experiment	Model	Experiment	Model
Western	5 s	112	99	83	68	85	87
Red	10 s	113	84	83	82	73	73
Cedar	15 s	160	126	120	82	99	74
Radiata	5 s	112	106	90	80	77	104
pine	10 s	137	125	97	94	78	86
	15 s	177	210	114	139	97	109
River Red	5 s	156	200	130	155	89	114
gum	10 s	182	195	153	175	90	116
	15 s	207	219	158	165	126	150

CONCLUSIONS

A numerical model based on a one-dimensional heat transfer and fully implicitly solution using tri-diagonal matrix has been developed to predict the re-ignition behavior of porous solid fuels. Generally speaking, the prediction of the model provides a good agreement with the experimental data. However, the model appears to be more accurate at higher levels of heat flux. As such, its range of applicability is limited to heat fluxes greater than 50 kW.m^{-2}. The change in key parameters, such as greater heat flux, results in lower differences between the experimental data and the calculation (model). It can be said that at higher heat flux, the shorter the ignition time and the higher the surface temperature and the inside temperature therefore the inner temperature gradient is very high. This is due to the heat accumulation absorbed by the sample surface.

REFERENCES

Ahmed, G.N. and Hurst, J.P. (1999). Modeling Pore Pressure, Moisture, and Temperature in High-Strength Concrete Columns Exposed to Fire, Fire Technology, Vol. 35, No. 3, 233-262.

Chase, C.A., Gidaspow, D., and Peck, R. E. (1970). Transient Heat and Mass Transfer in An Adiabatic Regenerator-A Green's Matrix Representation, Int. J. Heat mass transfer, Vol. 13, 817-833.

Dlugogorski, B.Z., Kennedy, E.M., and Hirunpraditkoon, S. (2004). Model Fires of Refuse Derived Fuels: Temperature Profiles and Pyrolysate Flux. 6th AOSFST, Daegu - Korea.

Hostikka, S. and McGrattan, K.B. (2001). Large Eddy Simulation of Wood Combustion. National Institute of Standards and Technology, Gaithersburg, MD 20899, USA.

Jiang, P.X. and Ren, Z.P. (2001). Numerical Investigation of Forced Convection Heat Transfer in Porous Media Using A Thermal Non-Equilibrium Model. International Journal of Heat and Fluid Flow, Vol. 22, Issue 1, 102-110.

Marafie, A. and Vafai, K. (2001). Analysis of Non-Darcian Effects on Temperature Differentials in Porous Media. International Journal of Heat and Mass Transfer, 44, 4401-4411.

Rubin, A. and Schweitzer, S. (1972). Heat Transfer in Porous Media with Phase Change. Int. J. Heat Mass Transfer, Vol. 15, 43-60.

Sahota, M.S. and Pagni, P.J. (1979). Heat and Mass Transfer in Porous Media Subjects to Fires. Int. J. Heat Mass Transfer, 22, 1069-1081.

Tien, H.C. and Chiang, K.S. (1999). Non-Darcy Flow and Heat Transfer in a Porous Insulation with Infiltration and Natural Convection. Journal of Marine Science and Technology, Vol. 7, no. 2, 125-131.

Tri Poespowati, Moghtaderi B, Dlugogorski BZ, Kennedy EM (2004). Pengaruh Porositas terhadap Karakteristik Re-ignition dari Surrogate Ceramic Under Flaming Conditions. Prosiding Seminar Nasional Fundamental dan Aplikasi Teknik Kimia 2004, Jurusan Teknik Kimia - ITS Surabaya.

Tri Poespowati (2006). Model Matematis Proses Re-ignition terhadap Material Berpori. Seminar Nasional Teknik Kimia Indonesia. Asosiasi Pendidikan Tinggi Teknik Kimia Palembang

Vafai, K. and Tien, C.L. (1981). Boundary and Inertia Effects on Flow and Heat Transfer in Porous Media. Int. J. Heat Mass Transfer, Vol. 24, 195-203.

Vynnycky, M. and Pop, I. (1997). Mixed Convection Due to A Finite Horizontal Flat Plate Embedded in A Porous Medium. J. Fluid Mech, Vol. 351, 359-378.